https://doi.org/10.5194/egusphere-2026-6782
Preprint. Discussion started: 22 November 2026
© Author(s) 2026. CC BY 4.0 License.

Role of ice sheet-ocean interactions in driving the current retreat of Northeast Greenland glaciers

Claudia Wekerle[1], Michael Wolovick[2], Yuting Dong[3], Martin Rückamp[4], Ralph Timmermann[1], and Torsten Kanzow[1,2]

[1]Alfred Wegener Institute, Helmholtz Centre for Polar and Marine Research, Bremerhaven, Germany
[2]University of Bremen, Bremen, Germany
[3]China University of Geosciences, School of Geography and Information Engineering, Wuhan, China
[4]Bavarian Academy of Science and Humanities, Munich, Germany

Correspondence: Claudia Wekerle (Claudia.Wekerle@awi.de)

Abstract.

The Northeast Greenland Ice Stream (NEGIS) drains through two major outlet glaciers with floating ice tongues: the 79 North Glacier (79NG) and Zachariæ Isstrøm (ZI). Since the 2000s, these glaciers have exhibited contrasting behavior: while the ZI ice tongue has retreated dramatically and transitioned to a tidewater glacier, the 79NG floating ice tongue has remained relatively stable in extent despite significant thinning. The retreat and thinning of both glaciers have accelerated the upstream ice stream, with important implications for global sea level rise. We present a novel coupled model that integrates the Ice-sheet and Sea-level System Model (ISSM) with the Finite volumE Sea Ice-Ocean Model version 2 (FESOM2). The ice sheet model domain encompasses the NEGIS region, while the global ocean model features enhanced mesh resolution on the Northeast Greenland continental shelf and explicitly resolves the cavities of both 79NG and ZI. This coupling enables dynamic representation of ice sheet-ocean-sea ice interactions, including grounding line migration and ice geometry evolution. A hindcast simulation spanning 2008-2021, forced by atmospheric reanalysis data, reproduces both the observed thinning at 79NG and the calving front retreat at ZI with good fidelity, validating our modeling approach. It reveals that mass loss from the 79NG floating ice tongue is dominated by basal melting, whereas at ZI it is dominated by iceberg calving. Our findings highlight the necessity of coupled ocean/ice sheet models for accurate future projections.

1 Introduction

Greenland's glaciers (both the inland ice sheet and peripheral ice caps) are major contributors to global sea-level rise, accounting for 17% (0.62 ± 0.06 mm yr^{-1}) of sea-level rise during the time period 2002–2021 (GlaMBIE Team, 2025). Ongoing mass loss of Greenland's glaciers varies from region to region. Draining around 11% of the Greenland Ice Sheet (Krieger et al., 2020), the Northeast Greenland Ice Stream (NEGIS) is the largest of Greenland's ice streams (Fig. 1a). In the last decades, it experienced accelerated ice flow, inland thinning, and sustained mass loss (Khan et al., 2022). It drains through two major outlet glaciers characterized by floating ice tongues: the 79 North Glacier (79NG, also Nioghalvfjerdsbræ) and Zachariæ Isstrøm (ZI), see Kanzow et al. (2025) for a review of the land, ice and ocean system. Both are prominent examples where two nearby

https://doi.org/10.5194/egusphere-2026-6782
Preprint. Discussion started: 22 November 2026
© Author(s) 2026. CC BY 4.0 License.

glaciers show a very different response to changes in glacier dynamics and ocean forcing. Whereas the 79NG has a floating ice tongue with an extent that has been relatively stable in recent years, the floating ice tongue of the ZI retreated since the 2000s and transitioned to a tidewater glacier (Mouginot et al., 2015).

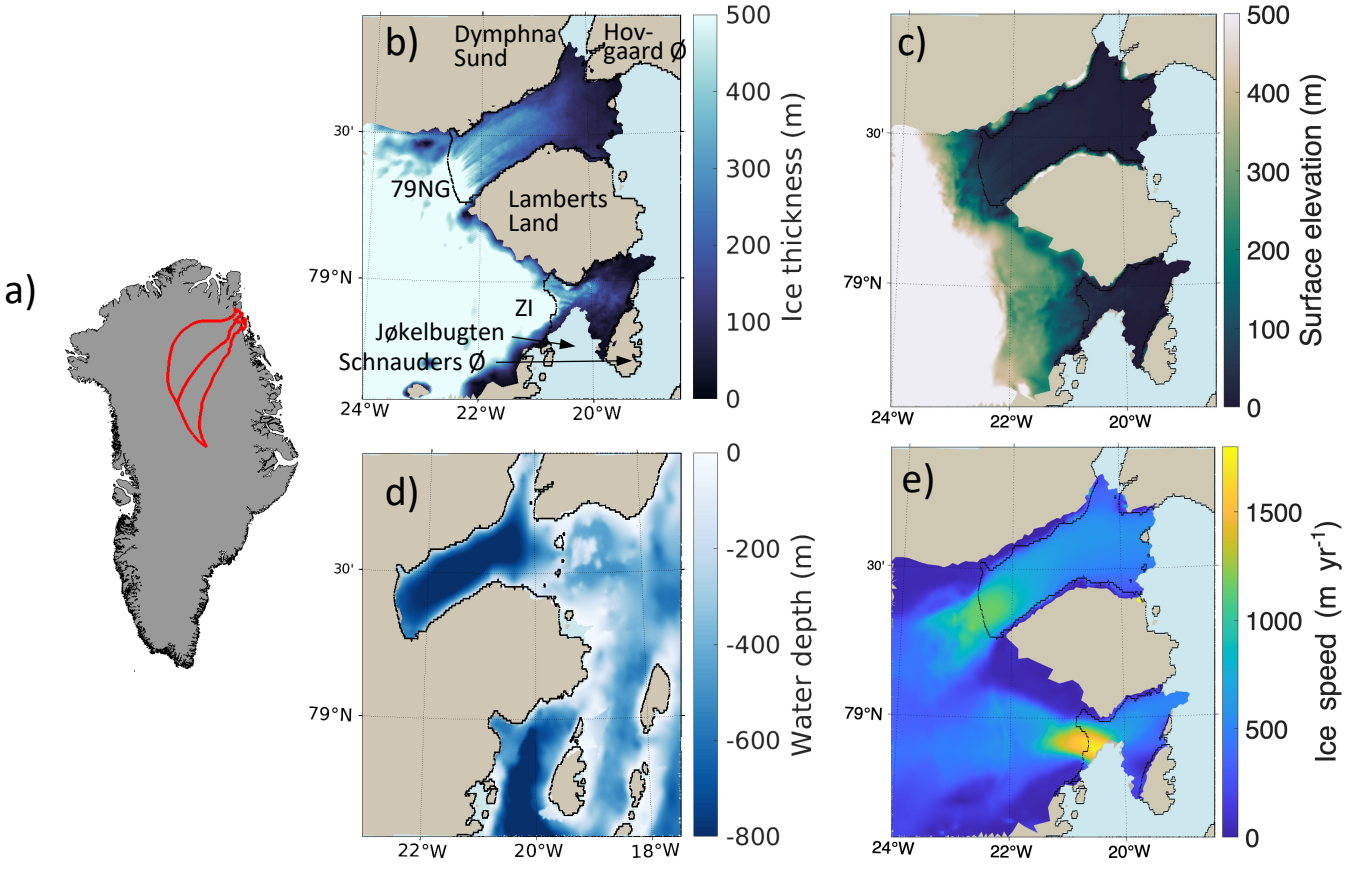


Figure 1. (a) Map of Greenland with catchment areas of 79NG and ZI in red, (b) ice thickness and (c) surface elevation from BedMachine Greenland v5 (Morlighem et al., 2017) and (d) water depth merged from RTopo-2.0.4 (Schaffer et al., 2019) and Oceans Melting Greenland (OMG, An et al., 2020) datasets. e) Ice speed from the ITS_LIVE dataset (Gardner et al., 2024) averaged from mid 2008 to mid 2009. Beige and light blue background colors indicate land and ocean, respectively.

The 79NG features an 80 km long ice tongue located in a narrow, around 20 km wide fjord. A bathymetric sill at its entrance suppresses the inflow of warm Atlantic Intermediate Water (AIW) into the cavity (Schaffer et al., 2020), and in addition, ice rises at the calving front exert a buttressing effect on the floating tongue. However, despite its relatively stable extent (except for an event in 2020 where parts of the floating ice in Dymphna Sund broke off; Humbert et al. (2023)), it has been thinning during the recent decade (Mayer et al., 2018; Zeising et al., 2024). Moreover, cracks at the eastern calving front developed that might be a precursor of instability of the floating tongue (Humbert et al., 2023). Wilson et al. (2017) showed that the negative mass balance of the 79NG ice tongue is determined by basal melting, driven by increased warm water flow into the cavity.

https://doi.org/10.5194/egusphere-2026-6782
Preprint. Discussion started: 22 November 2026
© Author(s) 2026. CC BY 4.0 License.

Here, the warming of the AIW layer on the Northeast Greenland continental shelf in the last decades comes into play (Schaffer et al., 2017; Gjelstrup et al., 2022), which resulted in increased heat transport into the cavity of the 79NG. However, there is also variability on shorter time scales overlaying the long-term trend, notably a cooling of the AIW inflow into the cavity since 2018 (McPherson et al., 2024).

The large scale warming of the AIW layer affected the ZI, located around 50 km south of the 79NG, as well. Between 2002 and 2014, the area of ZI covered by floating ice reduced by 95%, which caused the glacier to detach from a stabilizing sill and retreat rapidly along a downward-sloping, marine-based bed (Mouginot et al., 2015). In contrast to the 79NG, the floating ice of the ZI is not shielded by bathymetric sills. Furthermore, the breakup of the ZI ice tongue coincided with a reduction of ice mélange at the calving front (An et al., 2020). Ice mélange, a mixture of sea ice and icebergs, serves to stabilize the ice front and slows down glacier flow, as shown for Jakobshavn Isbræ by Amundson et al. (2010).

Modelling efforts have advanced our understanding of ocean-ice interactions at the 79NG. Mohammadi-Aragh et al. (2025) demonstrated based on a plume model how ice basal topography and the presence of basal channels influence basal melt rates. Reinert et al. (2026), employing a 3D ocean model with very high vertical resolution, revealed that basal melting is driven by three distinct subglacial plumes, shaped by ice topography and the Coriolis effect. Wekerle et al. (2024) applied a global ocean model with regional refinement that resolved the ocean circulation in the cavity of the 79NG, focusing on interannual time scales. Their study found that increased basal melting over the past two decades is mainly due to rising temperatures in the AIW layer, rather than increased subglacial discharge. Choi et al. (2017) used the Ice-sheet and Sea-level System model (ISSM) to simulate the future evolution of the NEGIS and its outlet glaciers based on simplified scenarios for basal and frontal melt. They suggested that the 79NG floating ice tongue would remain relatively stable over the next century, whereas ZI would lose its floating ice tongue completely. Using a different ISSM configuration, Dong et al. (2025) further investigated the sensitivity of glacier evolution to atmospheric and oceanic forcing and basal friction parameterizations. Their results indicated that 79NG could experience substantial thinning and grounding-line retreat, with potential instability along the ice-tongue margins even under low-emission scenarios.

Despite the knowledge gained from these simulations, ocean-only and ice sheet-only simulations do not account for feedbacks between the two components, which constitutes a large source of uncertainty especially for future projections. In particular, ocean-only simulations that resolve the cavity circulation of Greenland glaciers (e.g., Wekerle et al., 2024; Reinert et al., 2026) assume a static geometry of the ice tongue, a major drawback for future projections. Ice sheet models in turn rely on parameterizations of basal melt rates, e.g. based on far-field ocean temperatures that might not be realistic or ignore processes on the continental shelf or the sub-ice cavity. These limitations can only be overcome with coupled models. Here we present a coupled ocean-ice sheet model based on FESOM2 (Danilov et al., 2017) and ISSM (Larour et al., 2012) configured for the NEGIS region and its two outlet glaciers 79NG and ZI. The goal is to deepen our understanding of the significant changes observed at Northeast Greenland glaciers over the past two decades. We address two key questions: (1) Can we reproduce the distinct behavior of 79NG and ZI? (2) What drives these differences?

https://doi.org/10.5194/egusphere-2026-6782
Preprint. Discussion started: 22 November 2026
© Author(s) 2026. CC BY 4.0 License.

2 Methods

In this study we apply the coupled ocean-ice sheet model FESOM2-ISSM to study the dynamics of the Northeast Greenland glaciers. We first describe the individual models, then the coupling strategy and finally the experiments conducted in this study.

2.1 Ocean model

The Finite-volumE Sea ice-Ocean Model (FESOM2.5) is a global ocean/ice shelf/sea ice model which solves the standard set of hydrostatic primitive equations under the Boussinesq approximation with the finite volume method (Danilov et al., 2017). FESOM2.5 is formulated on unstructured meshes, allowing for mesh refinement in areas of interest. Details of the sea ice model were described by Danilov et al. (2015). The model resolves the ice shelf cavities of the Northeast Greenland glaciers (79NG and ZI). The interaction between ocean and ice shelf is simulated based on the three-equation system (Hellmer and Olbers, 1989). It computes melting and refreezing at the ice shelf-ocean boundary layer caused by velocity-dependent salt/heat exchanges. These basal melt rates are passed to the ice sheet model (see below). The model configuration used here is based on Wekerle et al. (2024). The background resolution of the computational mesh in the global oceans is set to 1° and refined to 25 km north of 40°N. In the Arctic Ocean and Nordic Seas, the mesh is refined to 4 km, and further refined to 2.5 km on the Northeast Greenland continental shelf. In the vicinity of the Northeast Greenland glaciers, mesh resolution is set to 700 m (Fig. 2b). For vertical discretization, 86 z-levels are used, with 5 m layer thickness in the top 100 m, and coarser layer thickness towards the ocean floor. The bathymetric data to generate the 3D mesh is taken from the RTopo-2.0.4 data set (Schaffer et al., 2019), merged with airborne gravity data from the Oceans Melting Greenland (OMG) mission in the region between ZI and Norske Trough from An et al. (2020) (Fig. 1d). To be consistent with the ice model, the initial ice topography of the ZI and 79NG ice tongues and bathymetry in initially grounded regions on Greenland is obtained from BedMachine Greenland version 5 (Morlighem et al., 2017) (Fig. 1b).

The ocean model is forced with atmospheric fields from the JRA55-do-v1.4.0 dataset (Tsujino et al., 2018), which has a spatial resolution of 55 km and temporal resolution of 3 hours. This dataset also includes river runoff, which we apply globally except for Greenland. Here instead, we use the datasets of solid ice and liquid freshwater runoff provided by Mankoff et al. (2020b) and Mankoff et al. (2020a), which have a higher temporal and spatial resolution than the JRA product. Another source of freshwater in the cavities of 79NG and ZI is the subglacial discharge. It results from surface melt on the ice sheet which drains through the ice and flows along the ice sheet base towards the grounding line of the floating ice tongues. To derive the subglacial discharge, we use the surface runoff field from the Regional Atmospheric Climate Model RACMO (Noël et al., 2019; Noël, 2019), which is summed up over the catchment areas of 79NG and ZI (red lines in Fig. 1b), i.e. upstream of the floating ice tongues. The subglacial discharge is then distributed equally over the grounding lines of 79NG and ZI. Note that the liquid runoff by Mankoff et al. (2020a) also includes runoff over the floating part of the glaciers, which overestimates the subglacial discharge injected at the grounding line of the ice tongues.

https://doi.org/10.5194/egusphere-2026-6782
Preprint. Discussion started: 22 November 2026
© Author(s) 2026. CC BY 4.0 License.

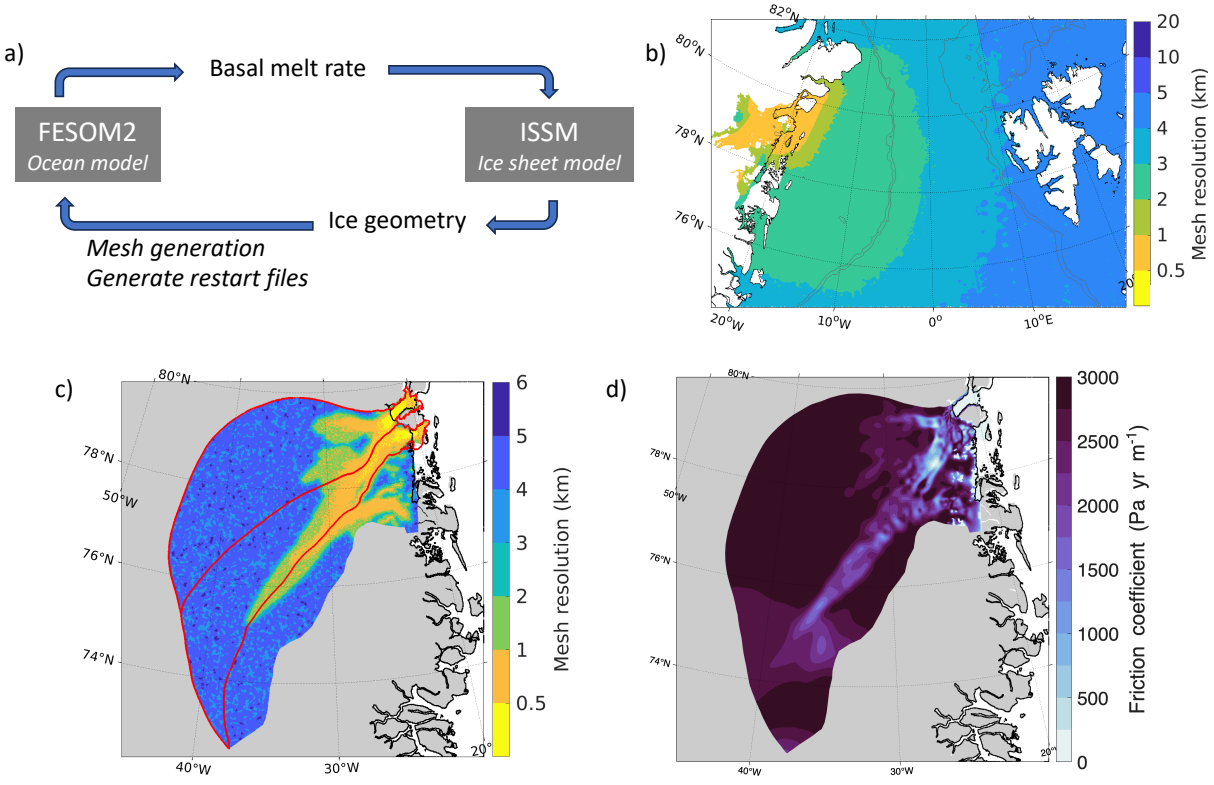


Figure 2. (a) Sketch illustrating the coupling procedure. (b) Resolution in km of the extended ocean model mesh. In every coupling step, inactive nodes are cut out of the extended mesh, resulting in a truncated mesh. The grey lines show the 500 m and 1000 m isobaths. (c) Resolution in km of the ice sheet model mesh. The red lines show the catchment areas of 79NG and ZI. (d) Inverted basal friction coefficient for grounded ice regions.

2.2 Ice sheet model

ISSM is an ice flow model based on the finite-element method (Larour et al., 2012). In this study, we use a model configuration comparable to the one presented by Dong et al. (2025), but with a slightly larger model domain. ISSM allows for unstructured meshes, similar to FESOM2. The mesh used in this study covers the domain of the NEGIS (Fig. 2c). The applied resolution follows the observed ice velocity and varies between 200 m in the region of the grounding lines and 5.5 km in regions where the ice moves slowly. The bed and surface ice topography is obtained from BedMachine Greenland version 5 (Morlighem et al., 2017) (Fig. 1c). The basal friction coefficient (Fig. 2d) was inferred using an inverse approach based on observed surface velocities from the MEaSUREs ITS_LIVE dataset from September 2008 to June 2009 (Gardner et al., 2024). The inversion employed the Shelfy-Stream Approximation (SSA, MacAyeal, 1989) and a Weertman friction law with an exponent of $m = 3$. The cost function combined velocity misfit and regularization terms, with the optimal regularization parameter determined through L-curve analysis (Wolovick et al., 2023).

https://doi.org/10.5194/egusphere-2026-6782
Preprint. Discussion started: 22 November 2026
© Author(s) 2026. CC BY 4.0 License.

To simulate the moving calving front, the von Mises calving scheme is used, where calving is proportional to the tensile stress regime at the ice front (Wilner et al., 2023). Retreat of the ice front (i.e. calving) occurs when the total tensile von Mises stress at the ice front exceeds a threshold σ_{max}, and advance occurs for values less than σ_{max}. Here we set this threshold to 1.5×10^5 Pa, consistent with the study by Choi et al. (2017). Moreover, we use level set-based moving boundaries (Bondzio et al., 2016). As in Choi et al. (2017), we apply a frontal melt rate that takes into account seasonal variability, parameterized as

$$\dot{M} = \dot{M}_{max} \frac{1 + \sin(2\pi t)}{2},$$

with $\dot{M}_{max} = 2\ \mathrm{m\,yr^{-1}}$ and t representing the day of the year. As atmospheric forcing, the annual mean surface mass balance from the Regional Atmospheric Climate Model (RACMO) is used (Noël et al., 2019).

2.3 Coupling strategy

The coupling between the ocean and ice sheet models follows a sequential approach with a coupling step of one year (Fig. 2a). In other words, ocean and ice components are run sequentially and with different time steps, but cover the same time span. First, the ocean model is integrated for one year. The simulated annual mean basal melt rates are passed to the ice model, which is then run for one year as well. The simulated ice shelf topography, i.e. ice draft and grounding line position, is then used to update the ocean mesh.

As there is no wetting-and-drying scheme available in FESOM2, we generated an "extended" 2D ocean mesh that incorporates areas upstream of the ice tongues that might become "ocean" in the future (Fig. 2b). In every coupling step, land nodes are cut out from the extended mesh and the ice draft of the cavities is corrected based on the ice shelf topography provided by the ice model. Similar to the concept developed by Timmermann and Goeller (2017), this results in a new "truncated" 2D ocean mesh. Then, a 3D ocean mesh is generated based on the prescribed number of z-levels.

In each coupling step the ocean model is restarted from its final state at the end of the previous coupling step. Ocean properties are thus remapped to the newly generated mesh, including extrapolation in areas where the ice has retreated. Similarly, the ice model is restarted from its previous final state. In case of retreating ice, basal melt rates are extrapolated to newly created cavity space. The simulated basal melt rates contain a slightly striped pattern due to the z-coordinate ocean mesh, and thus are smoothed with a variable-wavelength smoother before being passed to the ice model (Fig. A1).

2.4 Experiments

The FESOM2 simulation is initialized in 1990 with temperature and salinity fields from the PHC3 climatology (Steele et al., 2001) and run in stand-alone mode with prescribed cavity geometry for 18 years. The coupled FESOM2-ISSM simulation starts in 2008, in agreement with the imposed observed surface velocity field used in the inversion procedure. Moreover, the initial ice geometry used both in FESOM2 and ISSM is representative for the time around 2008 (Morlighem et al., 2017). This “hindcast” simulation is conducted until the year 2021. The time step of the ice sheet model is set to 0.05 yrs to satisfy the Courant-Friedrichs-Lewy condition. The ocean model runs with a time step of 3 min. One simulated year of the ocean model

https://doi.org/10.5194/egusphere-2026-6782
Preprint. Discussion started: 22 November 2026
© Author(s) 2026. CC BY 4.0 License.

takes about 9 h on 3456 processors, the ice sheet model takes 5 min, and the coupling script which includes preparation of the ice sheet and ocean models takes around 20 min.

To isolate the effect of the coupling procedure, we conducted a control run for the same time period with FESOM2 only, i.e. extending the spinup run until 2021. In this simulation, all model settings are kept the same as in the FESOM2-ISSM simulation, except that the cavity geometry is kept constant during the simulation.

In addition, sensitivity experiments with the ice sheet-only model are conducted to analyze the impact of ice tongue geometry and basal melt rate on the retreat of the ZI ice tongue. In these experiments, the ZI ice tongue is extended artificially to resemble 1990's conditions, setting ice thickness values to 80 m. Experiments with extended ZI ice tongue and reference conditions are conducted both without prescribed basal melt rate and with a melt rate of 30 m yr^{-1} at the grounding line that linearly decreases to zero at the calving front.

3 Results

We now present key results of the coupled ocean-ice sheet simulation. First, we analyze changes in the area and volume of the floating ice tongues (Sect. 3.1), which are directly linked to variations in ice speed, both for the floating and grounded ice (Sect. 3.2). We provide a mass balance assessment for both ice tongues (Sect. 3.3), and then examine basal melt rates and their connection to oceanic forcing (Sect. 3.4 and 3.5).

3.1 Area, thickness and volume changes of the floating ice tongues

Can the coupled model reproduce the observed retreat of 79NG and ZI? To answer this question, we now analyze calving front retreat as well as area, volume and thickness changes of both floating ice tongues, and compare to available observations. Fig. 3a shows the areas of the ice sheet model domain covered by floating and grounded ice, ice-free land and ocean at the beginning of the simulation. Subtracting the corresponding mask at the end of the simulation from the initial mask reveals the changes occurring during the simulation. Between 2008 and 2021, the grounding line at 79NG changes only slightly, it retreats by approximately 2 km (area shaded in orange), whereas the calving front remains nearly unchanged (Fig. 3b). This is consistent with the observed calving front by Millan et al. (2023) (Fig. 3d). In contrast, at ZI, the calving front retreats by approximately 10 km, even crossing parts of the former grounding line. This area is shaded in red, which shows a mask change from grounded ice to ocean (Fig. 3b). The simulated calving front retreat is however not as pronounced as in the observations (Fig. 3d). The observations show a detached floating ice fragment between Lamberts Land and Schnauders Ø, located in shallow waters (Fig. 1d), no longer connected to the ice sheet. In the simulation, there is still a narrow connection between the eastern and western parts of the ice tongue. At the start of the simulation, the 79NG and ZI ice tongues cover areas of 1620 km^2 and 690 km^2, respectively. After 14 years of simulation, the floating area of 79NG has decreased slightly by 1.8%, due to retreating floating ice in the western part of Dymphna Sund and at the southern margin close to the main calving front. At ZI, the floating ice area decreased substantially by 30%.

https://doi.org/10.5194/egusphere-2026-6782
Preprint. Discussion started: 22 November 2026
© Author(s) 2026. CC BY 4.0 License.

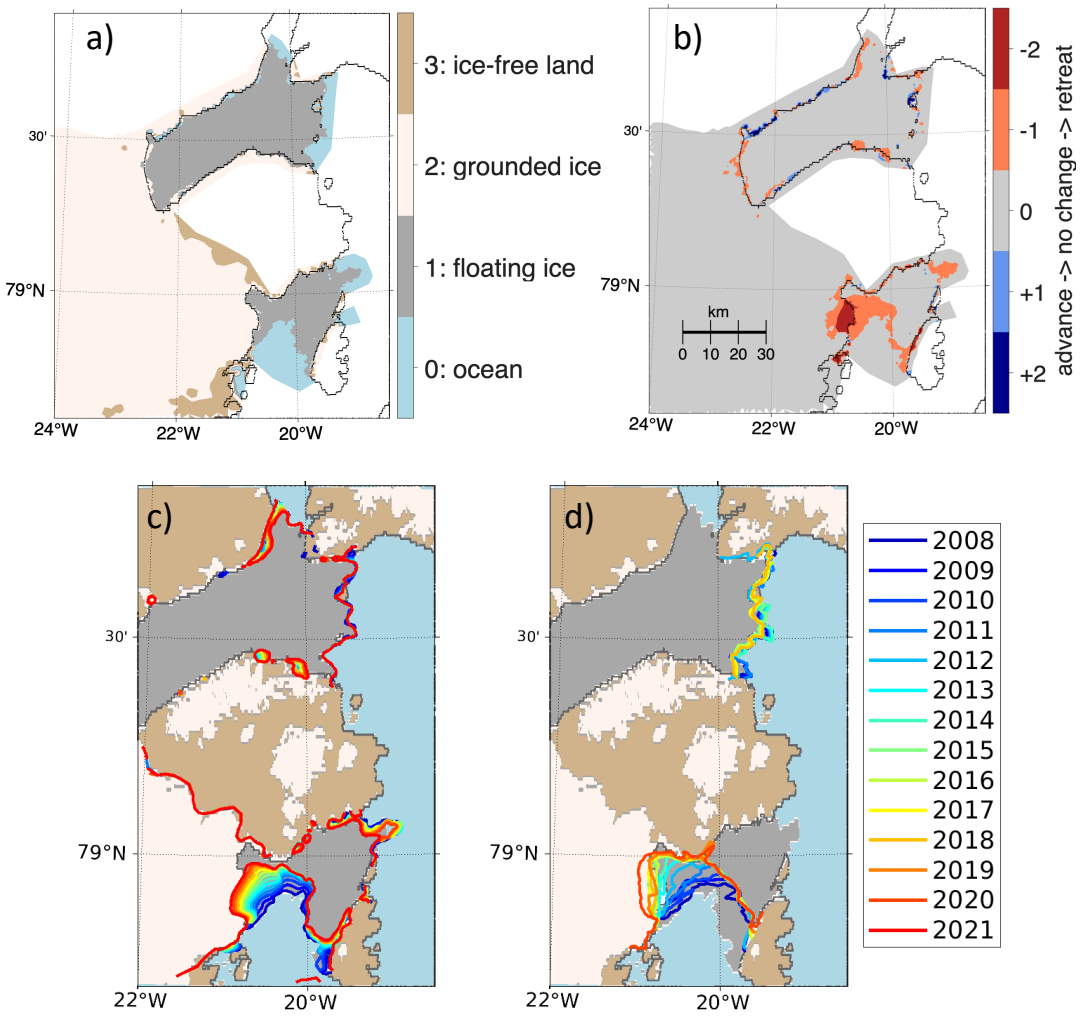


Figure 3. (a) Initial ISSM mask indicating ocean (0; blue), floating ice (1; grey), grounded ice (2; beige) and ice-free land (3; brown) at the start of the FESOM2-ISSM simulation in 2008. Note that the colored region shows the model domain. (b) Difference between the end and start of the simulation (2021 minus 2008). Orange areas indicate a transition from grounded ice to floating ice or from floating ice to ocean. Red areas indicate a transition from grounded ice to ocean. (c) Simulated and (d) observed (Millan et al., 2023) change of the calving fronts between 2008 and 2021. Note that the dataset ends in 2018 for 79NG.

Over the simulation period, the floating ice of 79NG thins (Fig. 4a), with the most pronounced thinning, up to 210 m, occurring in the south-western part of the cavity around 5 km away from the grounding line, where the ice initially exceeds 630 m in thickness. Notably, there is no thickness change near the calving front. How realistic is the simulated thinning of the 79NG ice tongue? It is substantially larger than an estimate derived from satellite-based elevation changes by Khan et al. (2022). However, stronger thinning has been reported in other observational studies. For example, Mayer et al. (2018) analyzed an ice ridge along the northern boundary of the floating ice and found thinning of nearly 30% between 1998 and 2016. Likewise,

https://doi.org/10.5194/egusphere-2026-6782
Preprint. Discussion started: 22 November 2026
© Author(s) 2026. CC BY 4.0 License.

using airborne radar measurements, Zeising et al. (2024) found a reduction in ice thickness of more than 50% approximately 10 km downstream of the grounding line between 1998 and 2018. Interestingly, almost no thickness change was observed between 2018 and 2021, coinciding with a notable cooling of the inflowing warm AIW (McPherson et al., 2024). Taken together, these observations suggest that our simulated thinning rate falls within the range of published estimates.

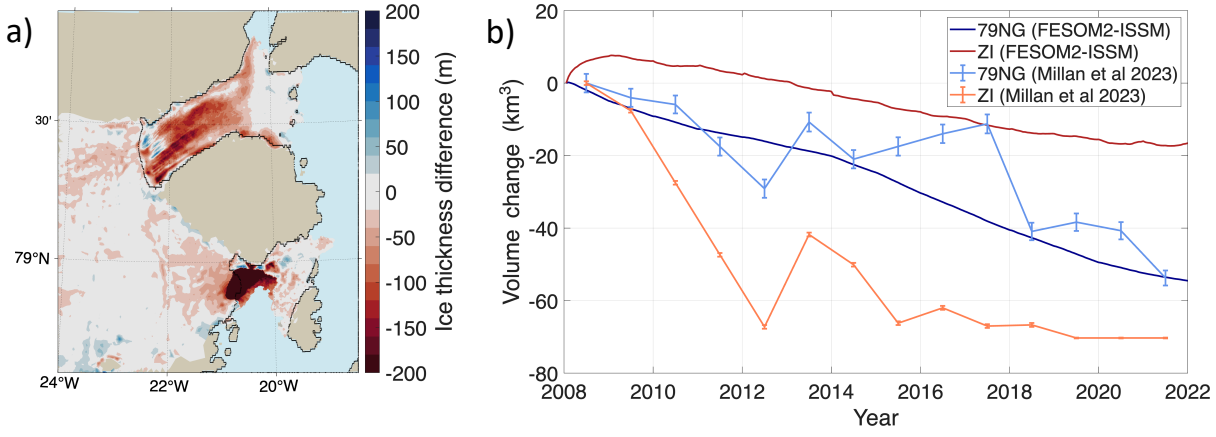


Figure 4. a) Ice thickness difference between the start and end of the FESOM2-ISSM simulation. (b) Time series of volume difference relative to the initial condition (1 January 2008) of the 79NG and ZI floating ice tongues simulated by FESOM2-ISSM (dark blue and red), and annual mean volume difference relative to the 2008 condition from the observation-based estimate by Millan et al. (2023) (light blue and orange).

The floating ice volume at 79NG decreases from 325 km^3 in 2008 to 270 km^3 by the end of 2021, a reduction of 17%. For comparison, Millan et al. (2023) reconstructed the volume change of the 79NG ice tongue using satellite-derived ice thickness data and estimated a similar volume loss over the same period (Fig. 4b). Unlike our simulation, their reconstruction suggests years of volume increase, particularly a notable rise between 2014 and 2017, a feature absent in our monotonic decline. Our simulation is more in line with Mayer et al. (2018) who found a monotonic thickness decrease of the 79NG floating ice.

At ZI, the floating ice volume changes by 19.5%, shifting from an initial 87 km^3 to 70 km^3 by the simulation's end. This volume decrease is much less than in the observational time series (-70 km^3), which shows an abrupt collapse between 2010–2012. The reason for this discrepancy between model and observations could be that the strong calving front retreat occurring until 2012 disconnected the western part of the ice tongue fed by inland ice from the eastern part located in shallower waters. In our simulation, these parts are not completely disconnected, the eastern part of the ice tongue thus still adds to the overall volume. Note that the eastern part of the floating ice initially holds a volume of around 50 km^3 in our model setup, which supports this hypothesis.

3.2 Ice speed changes of the outlet glaciers

We now investigate how the volume and thickness changes of the floating ice tongues described above translate into ice speed changes. The ice sheet model is initialized with ice velocities representative of 2008 conditions (see Methods). Initially, ice

https://doi.org/10.5194/egusphere-2026-6782
Preprint. Discussion started: 22 November 2026
© Author(s) 2026. CC BY 4.0 License.

speed is highest near the grounding line of 79NG, reaching 1170 $\mathrm{m\,yr^{-1}}$, while decelerating towards the calving front (Fig. 1e). By the end of the simulation, the flow of the floating ice of 79NG slows down by up to 350 $\mathrm{m\,yr^{-1}}$ (-60%) from about 20 km downstream of the grounding line toward the calving front (Fig. 5a). Near the grounding line, ice speed does not change much. At ZI, ice speed is highest close to the calving front with values up to 1740 $\mathrm{m\,yr^{-1}}$.

Over the 14-year simulation, the increase in ice speed at ZI is much higher than at 79NG (700 $\mathrm{m\,yr^{-1}}$, 45%). This speedup is also observed upstream of the glacier, it extends 30 km inland. The acceleration at ZI aligns with observed speed changes from the ITS_LIVE dataset (Fig. 5b). The changes in ice speed are related to changes in ice thickness described above. A decrease in ice thickness leads to a reduction in the backstress exerted by the floating ice on upstream grounded ice, which in turn increases the ice flux across the grounding line. Ice flow on the remaining eastern part of the ZI floating ice ceases due to reduced connectivity with the inland ice.

At 79NG, the ice speed decreases over the simulation period in the central and eastern parts of the floating ice tongue (Fig. 5a), a feature not evident in the available observations (Fig. 5b). For floating ice, the spreading rate depends strongly on ice thickness, and the deceleration occurs downstream of the simulated thinning (Fig. 4a). We therefore attribute the slowdown mainly to the evolving geometry. The discrepancy with observations likely arises because the simulated thinning is stronger than observational estimates (Khan et al., 2022) and more evenly distributed than in reality, where thinning is concentrated within basal channels (Zeising et al., 2024). The thicker ice between the channels may continue to sustain the ice flow. In addition, the ice rheology of the floating tongue is not constrained by the inversion, since the velocity misfit is restricted to grounded ice, which may also contribute to the mismatch.

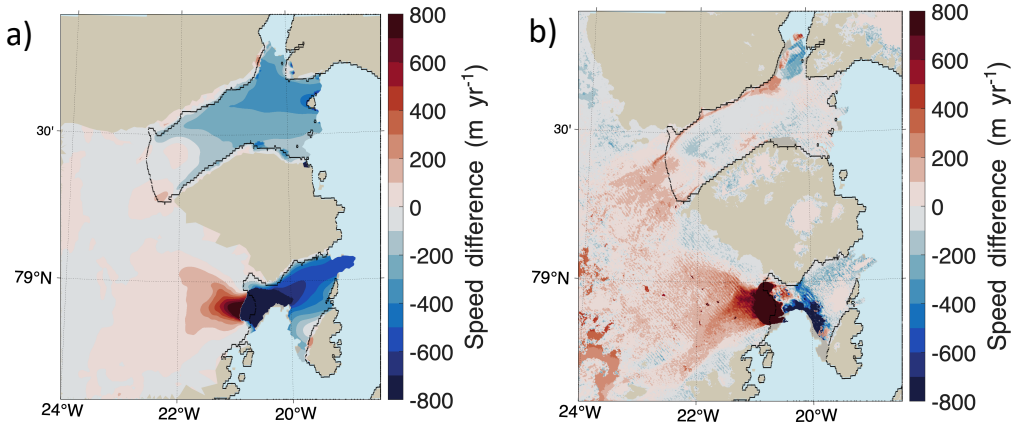


Figure 5. Ice speed difference between 2008 and 2021 (a) simulated by FESOM2-ISSM and (b) from measurements (ITS_LIVE, Gardner et al. (2024)).

https://doi.org/10.5194/egusphere-2026-6782
Preprint. Discussion started: 22 November 2026
© Author(s) 2026. CC BY 4.0 License.

3.3 Mass balance of the floating ice tongues

What are the primary drivers of mass loss of the Northeast Greenland major outlet glaciers? The surface mass balance (SMB) on the ice tongues contributes only minimally to the overall mass balance. In the ice sheet model, SMB is prescribed using data from the atmospheric model RACMO (Noël et al., 2019). Over the period 2008–2021, the integrated SMB averaged over areas with floating ice was 1.5 $Gt\,yr^{-1}$ for 79NG and 0.4 $Gt\,yr^{-1}$ for ZI (Fig. 6). The other two terms leading to mass loss of the floating ice tongues are basal melt and calving flux. Averaged over the time period 2008–2021, the relative contributions of basal melt and calving at 79NG are 95.5% (12.7 $Gt\,yr^{-1}$) and 4.5% (0.6 $Gt\,yr^{-1}$), respectively. The low calving flux can be explained by ice rises at the ice front that reduce the tensile stress facilitating calving. In contrast, at ZI basal melt is much lower than calving, here the relative contributions are 9% (1.7 $Gt\,yr^{-1}$) and 91% (17 $Gt\,yr^{-1}$), respectively.

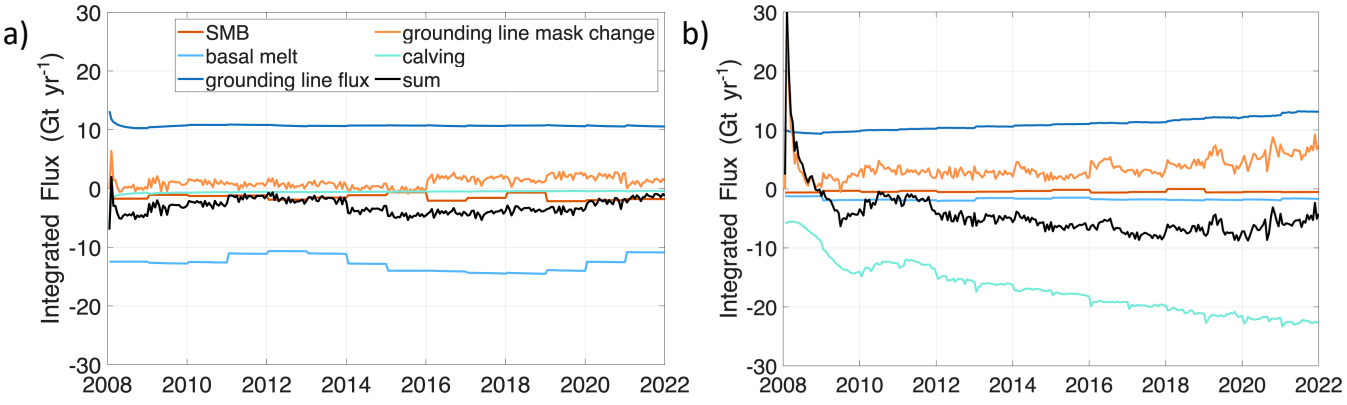


Figure 6. Floating ice mass budget computed by the ice sheet model for (a) 79NG and (b) ZI, showing the contributions of surface mass balance (SMB, red), basal melt (light blue), grounding line flux (blue), grounding line mask change (orange), calving (cyan), and the sum of all terms (black). Note that the ocean model passes annual mean basal melt rates to the ice sheet model.

The largest term counteracting the mass loss of the floating ice by surface and basal melt as well as calving is the ice flow across the grounding line. For the period 2009–2021 (i.e. excluding the first year of model adjustment), the mean grounding line flux is 10.7 $Gt\,yr^{-1}$ for 79NG and 11.1 $Gt\,yr^{-1}$ for ZI. For 79NG, the grounding line flux shows no significant trend over the 14-year simulation (Fig. 6a). This aligns with observations by Mouginot et al. (2015), reporting a stable grounding line flux of 11 $Gt\,yr^{-1}$ from 2002–2015. In contrast, for ZI their data show an increase from 11 $Gt\,yr^{-1}$ in 2002 to 15 $Gt\,yr^{-1}$ in 2015, which slightly exceeds but is consistent with our simulated rise from 9.4 $Gt\,yr^{-1}$ in 2009 to 13.1 $Gt\,yr^{-1}$ in 2021. Another term that contributes to the mass balance is the mass change resulting from the movement of the grounding line. It is computed as ice volume gained or lost from one time step to the next, normalized by the duration of that interval, and then converted into mass flux. Since the grounding line of ZI retreated inland throughout the simulation, this term is positive. Apart from the first year where an initial adjustment phase takes place, the floating ice tongues generally exhibit a negative mass balance. It amounts to -3.0 $Gt\,yr^{-1}$ and -5.3 $Gt\,yr^{-1}$ for 79NG and ZI, respectively. As shown above, for 79NG, basal melt dominates the mass

https://doi.org/10.5194/egusphere-2026-6782
Preprint. Discussion started: 22 November 2026
© Author(s) 2026. CC BY 4.0 License.

balance. The following subsection explores the variability of basal melt over the 14-year simulation period and its relationship with oceanic forcing.

3.4 Role of ocean forcing for the basal melt rates of the 79NG ice tongue

We first analyze the spatial pattern of basal melt rates. In 2008, at the start of the coupled simulation, the simulated melt rates beneath the 79NG floating ice tongue are highest near the grounding line with values up to 53 $\mathrm{m\,yr^{-1}}$ (Fig. 7a), where the ice is thickest (Fig. 1b). At ZI, basal melt rates are much lower than at 79NG, and are concentrated in areas with thick ice and deeper water, enabling contact with the warm AIW found at the bottom of the water column. After 14 years of simulation, the basal melt rates in the central part of 79NG have decreased and become more localized near the grounding line, with values up to 88 $\mathrm{m\,yr^{-1}}$ (Fig. 7b). Comparing the simulated basal melt pattern of 79NG with observations from Millan et al. (2023), we find an overall good agreement, although observed melt rates are more localized near the grounding line (Fig. 7c). The cavity-integrated basal melt rate simulated by FESOM2-ISSM amounts to 13.2 $\mathrm{km^3\,yr^{-1}}$ for 2008–2021, which is slightly lower than but within the error margins of the observational estimates of 17.8±5.2 $\mathrm{km^3\,yr^{-1}}$ for the years 2016–2017 (Schaffer et al., 2020) and 14.2±0.96 $\mathrm{km^3\,yr^{-1}}$ for the years 2011–2015 (Wilson et al., 2017).

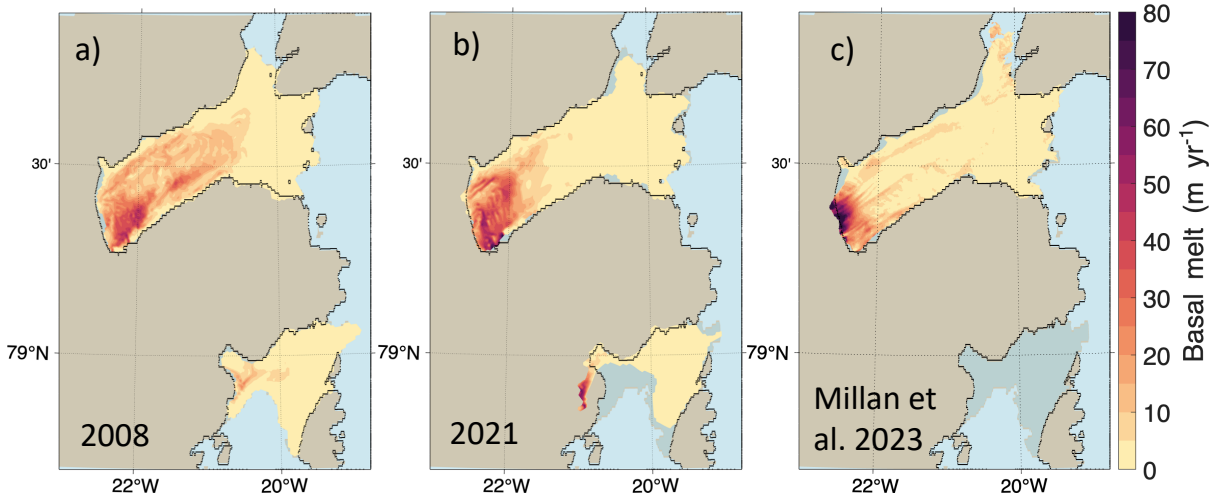


Figure 7. Simulated basal melt rate (a) in 2008 and (b) in 2021. (c) Observed basal melt rate of the 79NG floating ice tongue from Millan et al. (2023) (averaged over the years 2002–2020). Note that melt rates from Millan et al. (2023) are only available for the 79NG, and not for ZI.

Previous studies showed that the primary driver of basal melt is the inflow of warm and salty AIW into the cavity of 79NG (Wekerle et al., 2024). The water column on the Northeast Greenland continental shelf, the source region of the AIW, is strongly stratified. Here, cold and fresh Polar Water (PW) overlies the dense, warm, and salty AIW. The AIW itself originates from Atlantic Water that recirculated in Fram Strait and entered the continental shelf, as well as from colder Arctic Atlantic Water that circulated through the Arctic Ocean (McPherson et al., 2023). Mooring observations at the 79NG calving front reveal

https://doi.org/10.5194/egusphere-2026-6782
Preprint. Discussion started: 22 November 2026
© Author(s) 2026. CC BY 4.0 License.

pronounced interannual variability in AIW properties, with temperatures increasing from 2016 to 2018 and then decreasing until 2021 (McPherson et al., 2024). Our simulation reproduces this pattern, although with a weaker decrease in temperatures from 2018 onwards (Fig. 8). Nonetheless the simulated AIW temperatures are around 0.3–0.5°C warmer than the mooring-based observations, a warm bias already present in the ocean-only simulation described by Wekerle et al. (2024). We now analyze the connection between changes in AIW temperatures and basal melt rate in the coupled model.

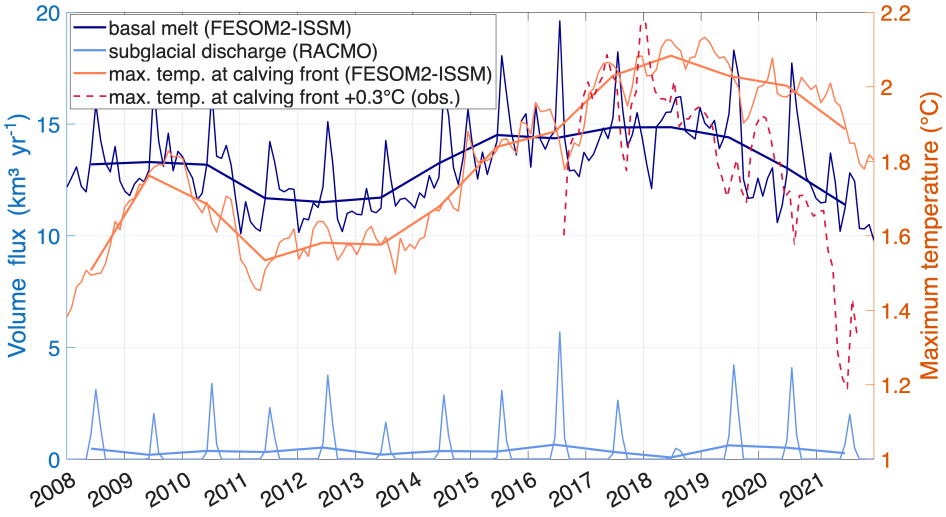


Figure 8. Time series of basal melt rate of the 79NG ice tongue (dark blue), subglacial discharge at 79NG derived from RACMO runoff fields (light blue), maximum temperature in the water column at the calving front of 79NG simulated by FESOM2-ISSM (orange) and measured by moorings deployed at the 79NG calving front (red line, with an offset of 0.3°C, McPherson et al. (2024)). Annual and monthly means are shown by thick and thin lines respectively.

Annual mean basal melt rates correlate significantly with the maximum AIW temperature at the calving front (r = 0.83), whereas the correlation with annual mean subglacial discharge is not significant (r = 0.07). Note that all time series were detrended before the correlations were computed. The annual mean time series shows a decrease in basal melt rates from 2018 onward, which is consistent with the decrease in melt rates near the grounding line of 79NG observed by McPherson et al. (2024). On monthly time scales, however, basal melt rates correlate significantly with both AIW temperature (r = 0.60) and subglacial discharge (r = 0.61). This suggests that subglacial discharge imprints on basal melt rates on seasonal time scales, while interannual variability is controlled by AIW temperature. The year 2018 illustrates this: basal melt rates stayed low even in the summer months, because exceptionally cold air temperatures (Kanzow et al., 2025, their Fig. 6) reduced the subglacial discharge into the cavity.

3.5 Role of ocean forcing and ice tongue geometry for the retreat of the ZI ice tongue

We now examine the simulated retreat of the ZI ice tongue more closely. To assess the role of ocean forcing in this retreat, we performed a sensitivity experiment using the ice sheet model only, and artificially setting the basal melt rate to zero.

https://doi.org/10.5194/egusphere-2026-6782
Preprint. Discussion started: 22 November 2026
© Author(s) 2026. CC BY 4.0 License.

Additionally, we ran a simulation where the basal melt rate increased linearly from 0 m yr^{-1} at the calving front to 30 m yr^{-1} at the grounding line. Both simulations cover the period 2008–2021 and start from the same initial conditions as the coupled run. Our results show that even without basal melt, the floating ice retreats, with a calving front nearly identical to that of the run with prescribed basal melt (Fig. 9b,c). Volume change, calving fluxes, and grounding line flux exhibit only minor differences (blue solid and dashed lines; Fig. 9g,h,i). This suggests that at the start of the simulations, the floating ice of ZI is already in a state of retreat that further proceeds independent of oceanic forcing.

We started both our coupled simulation and the ISSM-only simulations in 2008, as the most commonly used ice shelf thickness data (BedMachine v.5; Morlighem et al. (2017)) are representative of that year. However, the retreat of the ZI ice tongue began several years earlier. Mouginot et al. (2015) showed that increased discharge across the grounding line already occurred in 2002. Consequently, it is plausible to assume that the floating ice geometry we prescribed in our simulations (Fig. 1b) does not represent an equilibrium state. The notch on the southern side of the floating ice creates an environment with exceptionally high tensile stresses and minimal buttressing, resulting in strong calving fluxes (Fig. 9h). Since calving is primarily governed by the stress state near the glacier front, it is an ice sheet-internally controlled process in our simulations. As long as stress conditions at the terminus exceed the calving criterion, frontal retreat can proceed, even without basal melting. In contrast, the 79NG features a more "classic" ice shelf geometry: an elongated flow within a confining fjord, with buttressing provided by rock walls on both sides, as well as ice rises and small islands near the calving front. This configuration makes 79NG more stable, and more sensitive to oceanic forcings.

To further investigate the influence of ice tongue shape on glacier retreat, we conducted additional ISSM-only experiments. In these, we artificially enlarged the ZI ice tongue to resemble its 1990s geometry (Millan et al., 2023), setting the ice thickness in the newly added area to 80 m (Fig. 9d). As before, we ran two experiments: one with basal melt set to zero and another with a linear increase from 0 to 30 m yr^{-1} at the grounding line. In both enlarged-ice-tongue experiments, the floating ice volume increases markedly until 2018 and declines slightly thereafter; a feature even more pronounced in the experiment without basal melt (red lines in Fig. 9g). The volume increase reflects a thickening of the central ice tongue by more than 200 m by the end of the simulations (Fig. 9e,f). Almost no calving occurs until 2016, after which it increases gradually (Fig. 9h). The grounding line flux remains stable in both enlarged-ice-tongue experiments, whereas in the simulations with prescribed 2008 ice geometry it increases steadily from 10 Gt yr^{-1} to 15–16 Gt yr^{-1}. This shows that the enlarged ice tongue buttresses the upstream ice. The enlarged-ice-tongue experiments with and without prescribed basal melt differ in ice volume, thickness and calving. This indicates that oceanic forcing contributes to the initial retreat of the enlarged ZI ice tongue.

4 Discussion

4.1 Strengths of the coupled framework

The coupled framework is able to represent the contrasting behaviour of the two major Northeast Greenland glaciers. This is consistent with observations from other floating ice tongues in North Greenland, which have thinned substantially in recent decades. At Petermann Glacier, the loss of about 40 km of its ice tongue in 2010 and 2012 caused only a minor acceleration,

https://doi.org/10.5194/egusphere-2026-6782
Preprint. Discussion started: 22 November 2026
© Author(s) 2026. CC BY 4.0 License.

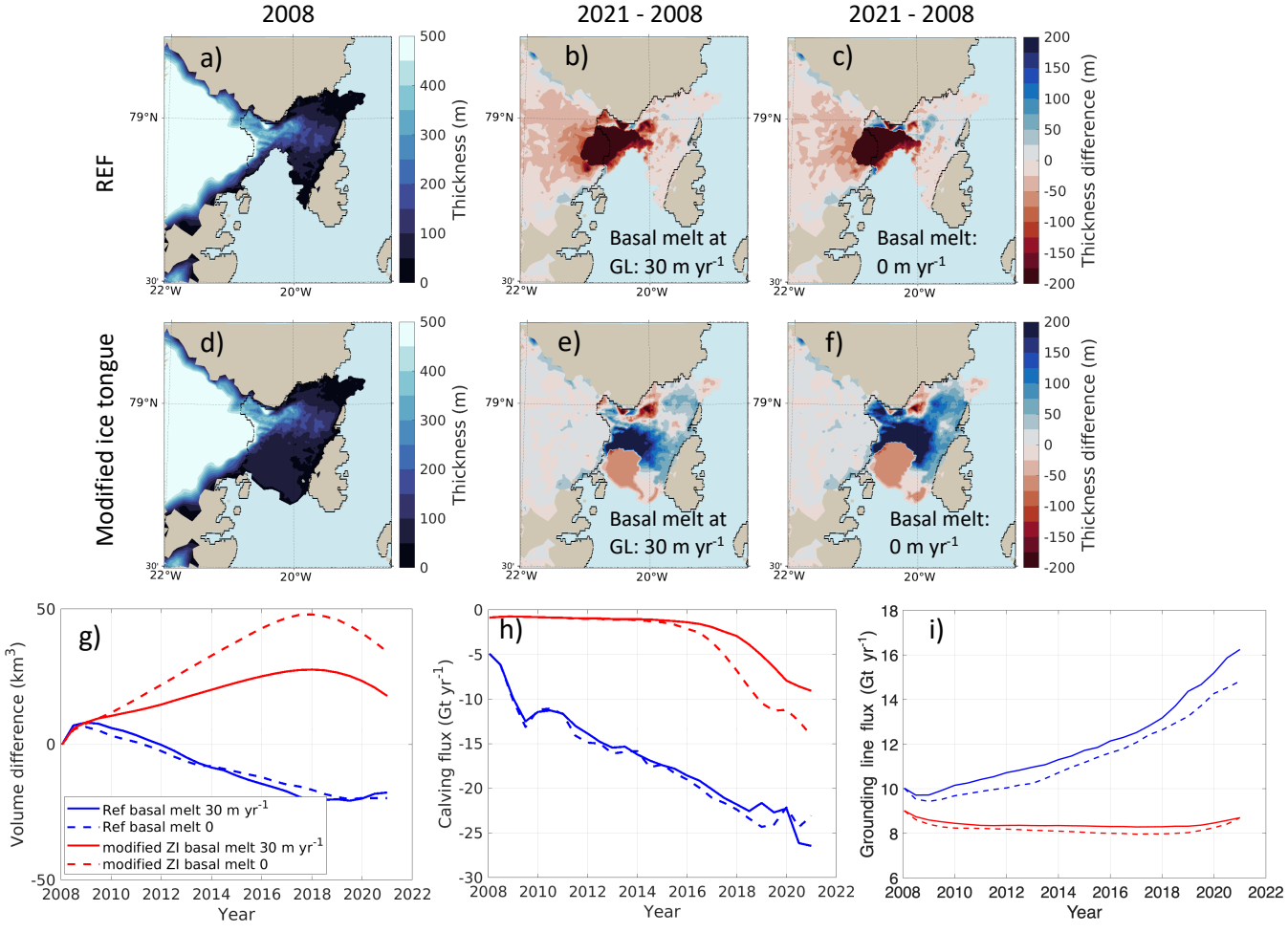


Figure 9. ISSM-only experiments analyzing the sensitivity of ZI to basal melt and ice tongue shape. Panels (a,d) show ice thickness at the start of the simulation (2008), while (b,c,e,f) show the difference between 2008 and 2021. The first row presents results for experiments using the reference ice shelf geometry, and the second row for those using a modified geometry resembling 1990s conditions (ice thickness is set to 80 m in the added ice tongue area). The middle column shows experiments with a prescribed basal melt rate of 30 m a^{-1} at the grounding line, and the right column shows experiments with no basal melt. Time series of (g) volume difference relative to the initial condition (1 January 2008), (h) calving flux, and (i) grounding line flux are shown for all four experiments: blue and red lines represent experiments starting from reference and modified ice shelf geometries, respectively, while solid and dashed lines indicate moderate basal melt and zero basal melt, respectively.

295 because the thin distal ice calved off provided little buttressing, whereas calving closer than about 12 km to the grounding line is expected to cause a strong dynamic response (Hill et al., 2017; Rückamp et al., 2019). Similar to our ZI experiments, this indicates that the sensitivity of a glacier depends less on the total ice loss than on ice loss close to the calving front / pinning points. Like ZI, the C. H. Ostenfeld ice tongue in North Greenland collapsed in 2002, most probably because Atlantic Water

https://doi.org/10.5194/egusphere-2026-6782
Preprint. Discussion started: 22 November 2026
© Author(s) 2026. CC BY 4.0 License.

could flow unimpeded into its cavity (Jakobsson et al., 2026). In contrast, the neighbouring Ryder Glacier is shielded by a bathymetric sill that restricts the inflow of warm water, which has kept the glacier stable so far (Jakobsson et al., 2020).

As described above, bathymetry and topography play a large role for the stability of glaciers. A key strength of both the ice sheet and ocean model is their multi-resolution approach. The 200 m resolution of the ice sheet model allows us to represent grounding line migration and friction along the fjord walls, and to resolve important features such as ice rises at the 79NG calving front, which turn out to be a key feature for the contrasting behaviour of the two outlet glaciers. The multi-resolution ocean model bridges scales from the local to the regional and global. At small scales, it resolves the inflow of warm AIW into the 79NG cavity through a narrow trough and faithfully represents bathymetric features such as sills that constrain this inflow. At larger scales, it simulates regional ocean conditions, in particular the circulation of Atlantic Water in the Nordic Seas and its westward recirculation in Fram Strait, which provides realistic boundary conditions for the cavity inflow.

The main benefit of coupling, compared to the ocean-only simulations of Wekerle et al. (2024), is that cavity geometry and melt rates evolve together. At 79NG, the ice draft near the grounding line reduces by up to 210 m over 14 years in our simulation, and the melt maximum becomes more concentrated near the grounding line. A static-geometry ocean model cannot capture this redistribution, as shown by a comparison of FESOM2-ISSM with a FESOM2 control run based on static cavity geometry (Fig. 10a,b). The water column on the Northeast Greenland continental shelf is strongly stratified, with warm, salty Atlantic-origin water at depth beneath a layer of cold, fresh PW. As the ice tongue thins, its base migrates upward from the warm AW to the cold PW which reduces basal melting. This phenomenon creates a negative feedback mechanism for basal melt, and has been observed for Antarctic ice shelves as well (Paolo et al., 2023). In line with this, the FESOM2-ISSM simulation reveals a decrease in basal melt rate of 13% in the second half of the simulation compared to the FESOM2-only simulation (Fig. 10c). In addition, it has to be taken into account that the changing ice draft changes the pressure-dependent freezing point (e.g. Holland and Jenkins, 1999) and the plume dynamics (e.g. Jenkins, 2011).

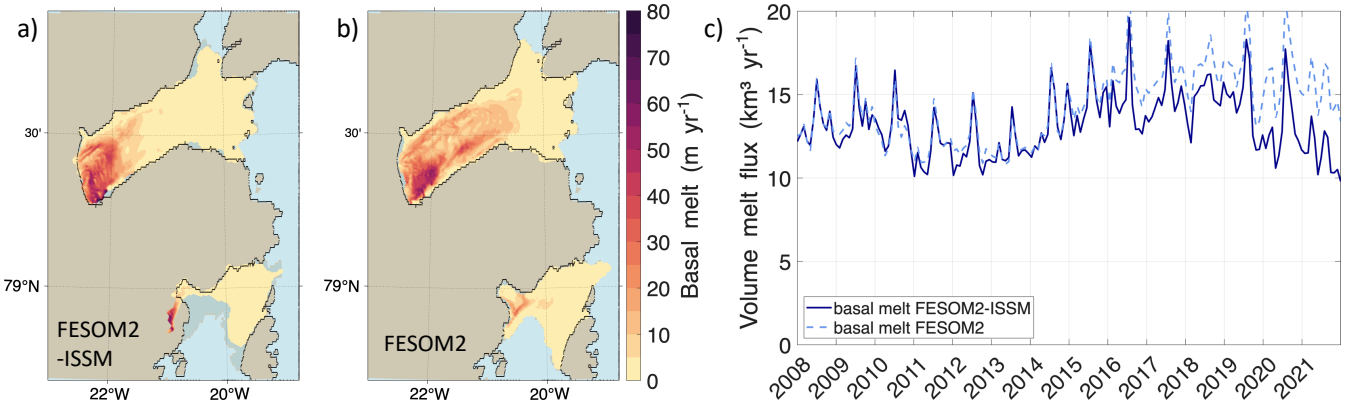


Figure 10. Basal melt averaged over the year 2021 simulated by (a) FESOM2-ISSM with evolving ice tongue geometry and (b) FESOM2 with static ice tongue geometry. (c) Time series of monthly mean integrated basal melt of the 79NG ice tongue simulated by FESOM2-ISSM (blue line) and FESOM2 (light blue dashed line).

https://doi.org/10.5194/egusphere-2026-6782
Preprint. Discussion started: 22 November 2026
© Author(s) 2026. CC BY 4.0 License.

Conversely, ice sheet-only studies of the NEGIS outlet glaciers (Choi et al., 2017; Dong et al., 2025) had to rely on prescribed or parameterized basal melt. Our results show that interannual melt variability at 79NG follows AIW temperature at the calving front (r = 0.83), while subglacial discharge mainly modulates melt on seasonal time scales. Simple parameterizations based on, e.g. far-field ocean temperature, can only partly capture this separation of time scales. The coupled simulation could therefore serve as a benchmark for evaluating such parameterizations in a Greenland fjord setting.

4.2 Limitations of the coupling strategy and the ice sheet and ocean model setups

The sequential coupling with an annual time step means the ice sheet model is forced with annual mean basal melt rates. The ocean in turn sees a cavity geometry that stays fixed for one year. Given the moderate geometry changes per year at 79NG, this is likely a reasonable approximation. Coupling intervals and their effect on numerical stability and results have been studied in idealized coupled setups (e.g. Asay-Davis et al., 2016; Jordan et al., 2018; Gladstone et al., 2021). Seasonal variability of basal melt, which correlates significantly with subglacial discharge on monthly time scales, is however not passed to the ice sheet model. Whether a seasonal melt peak could in principle cause irreversible changes could be tested with shorter coupling intervals. Given the large ice thickness near the 79NG grounding line, we expect this effect to be small.

Both cavity grounding zones are regions of highest melt. How melt is applied to partially floating elements in ISSM can strongly affect grounding line migration (Seroussi and Morlighem, 2018). Here we use the sub-element melt option where basal melt is applied on elements that cross the grounding line by scaling with the floating area fraction of each partially floating element. This choice should ideally be tested for sensitivity. In addition, melt rates are extrapolated into newly opened cavity space after retreat. This may misrepresent melt in the first year of exposure, especially where new cavity space opens close to the grounding line.

On the ice side, we use the SSA, which neglects vertical shear. This is justified for floating ice and fast-flowing ice streams, but less accurate in slow-moving parts of the catchment and at grounding zones with steep bedrock. The basal friction field comes from an inversion against 2008-2009 velocities using a non-linear Weertman law ($m = 3$), and it stays fixed during the simulation. Dong et al. (2025) showed that future projections for 79NG and ZI are sensitive to the friction law. Compared with regularized Coulomb laws, a Weertman law tends to underestimate the upstream response to changes in buttressing (e.g., Brondex et al., 2017; Joughin et al., 2019). The simulated inland acceleration at ZI (~ 30 km) may therefore be a lower bound. The first-year adjustment in the mass budget also shows that the initial state is not fully in balance with the forcing. This is a known problem in ice sheet initialization and should be kept in mind when interpreting trends in the first years.

Surface mass balance and subglacial discharge are both taken from RACMO and are not coupled to the evolving ice geometry or to a subglacial hydrology model. Over a 14-year hindcast this is acceptable. For centennial projections, the feedback between surface lowering and surface melt, and the evolving drainage of meltwater toward the grounding line, may become important.

At ZI, mass loss is dominated by calving. In our model setup, calving is represented by the von Mises calving law. The simulated calving front retreat is slightly weaker than observed (Fig. 3). A systematic comparison of different calving laws, as done by Choi et al. (2018) for other Greenland glaciers, might improve the model in the future. Furthermore, a process not taken into account in ISSM is the presence of ice mélange and landfast ice. The southern part of the ZI floating ice that

https://doi.org/10.5194/egusphere-2026-6782
Preprint. Discussion started: 22 November 2026
© Author(s) 2026. CC BY 4.0 License.

flows into Jøkelbugten can be described as a heterogenous ensemble of ice blocks glued by an ice mélange (An et al., 2020). As summarized by Reeh et al. (2001), ice mélange at the calving front of a glacier may apply sufficient back-pressure to prevent crevasse formation and/or propagation and keep together the partly or fully disintegrated frontal region of the glacier, preventing icebergs from drifting away. Lippert et al. (2025), based on ISSM simulations for Kangerlussuaq Glacier, found that changes in the maximum tensile stress threshold precedes changes in ice mélange, suggesting to account for variations in calving parameters during the simulation, an approach that could be tested for ZI as well.

At 79NG, mass loss is dominated by basal melt. The cavity-integrated melt rate ($13.2\,\mathrm{km^3\,yr^{-1}}$) lies within the uncertainty of the observational estimates (Wilson et al., 2017; Schaffer et al., 2020) and the spatial pattern agrees well with Millan et al. (2023). However, this agreement could be partly due to errors that cancel each other out. The simulated AIW at the calving front is 0.3–0.5°C warmer than observed, which in itself would promote excessive melting. At the same time, several processes known to enhance melting are either missing or only roughly represented. Based on a plume model, Mohammadi-Aragh et al. (2025) recently showed that basal channels, in particular in the hinge zone close to the grounding line, exert a dominant control on basal melt rates. In our ocean model, the ice draft is taken from BedMachine v.5 (Morlighem et al., 2017), which does not explicitly resolve these channels. Moreover, Zeising et al. (2024) showed that the recent thinning of the 79NG ice tongue occurred predominantly within the channels, so not resolving them might lead to an underestimate of basal melt rates.

Another limitation concerns subglacial discharge, which our ocean model injects evenly along the grounding line. Model experiments for an Antarctic ice shelf show that the location of the injection changes the amount of basal melt (Jesse et al., 2026). Injecting subglacial discharge at point sources such as basal channels could therefore modify the simulated basal melt rates.

5 Conclusions

Here, we present a novel modeling framework that couples two high-resolution models: the ice sheet model ISSM and the ocean/ice shelf/sea ice model FESOM2. Focused on the Northeast Greenland Ice Stream and its two major outlet glaciers, 79NG and ZI, the model configuration has been extensively validated against observational data, demonstrating overall strong performance. Observations indicate that basal melt rates at 79NG are currently too high for the ice tongue to remain in equilibrium (Wilson et al., 2017; Millan et al., 2023). Consistent with this, our simulation shows a negative mass balance of the floating ice tongue for 2008–2021, with mass loss dominated by basal melting. On interannual time scales, basal melt is controlled by oceanic forcing, in particular the temperature of AIW, whereas on seasonal time scales the injection of subglacial discharge into the cavity at the grounding line equally contributes.

Regarding the ZI, our results indicate that the recent ice tongue retreat is rather driven by its unstable geometry, featuring a notch that reduces buttressing and promotes calving, than by oceanic forcing, as shown by simulations where retreat continues even without basal melt. When we artificially restore the ice tongue to its 1990s extent, thickening and delayed calving demonstrate its buttressing effect, stabilizing upstream ice and grounding line flux. In contrast, the 2008 geometry lacks this support, leading to a steady increase in ice discharge across the grounding line right from the start of the model integration. The ocean

https://doi.org/10.5194/egusphere-2026-6782
Preprint. Discussion started: 22 November 2026
© Author(s) 2026. CC BY 4.0 License.

may still have played an important role: one can speculate that the warming of AIW since the 2000s increased ocean-driven melt and thereby led to an initial instability of ZI, after which glacier dynamics took over and the glacier entered a mode of ongoing retreat.

Next, the model setup presented here can be used to conduct future projection scenarios. This will allow us to better understand the future evolution of Northeast Greenland's glaciers: How far inland will the ZI retreat until the end of the century under different climate scenarios? Will the 79NG ice tongue disintegrate in the future? What will be the corresponding sea level contribution? Existing ice sheet-only simulations showed that 79NG could experience substantial thinning and grounding-line retreat over the next century (Dong et al., 2025). In the high-emission scenarios described by Dong et al. (2025), the combined sea level contribution of 79NG and ZI is about 3 mm by 2100, mainly driven by atmospheric warming. These projections rely on prescribed ocean forcing, which cannot respond to the changing ice draft and cavity geometry. In our coupled setup, basal melt evolves with the cavity, so the ocean-driven part of the projected retreat, and the uncertainty it adds, can be quantified.

Code and data availability. The FESOM2 source code is available at https://github.com/FESOM/fesom2. We used version FESOM2.5.2. Documentation of the source code and how to run the model can be found here: https://fesom2.readthedocs.io/en/latest/index.html. The ISSM source code is available at https://issm.jpl.nasa.gov (Larour et al., 2012). Here we used ISSM version 4.22. Simulation results are available at https://doi.org/10.5281/zenodo.23861634 (Wekerle, 2026).

Appendix A: Supplementary figures

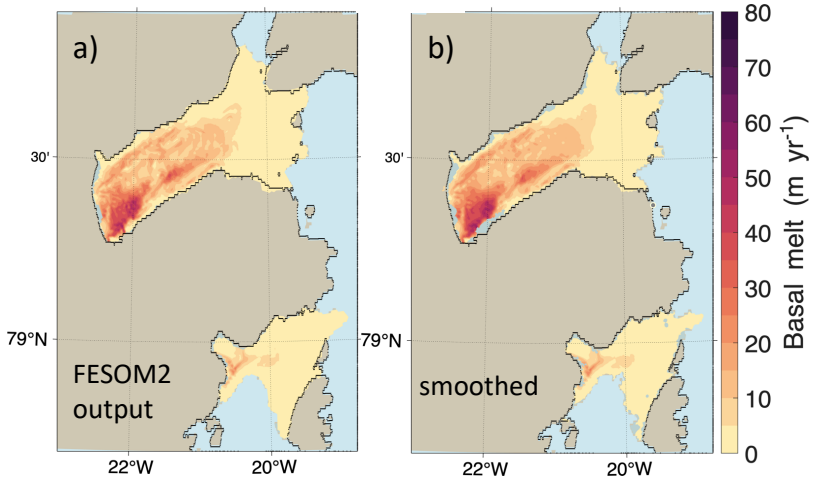


Figure A1. Basal melt averaged over the year 2008 (a) simulated by FESOM2-ISSM and (b) the same field, but smoothed used as input for ISSM.

https://doi.org/10.5194/egusphere-2026-6782
Preprint. Discussion started: 22 November 2026
© Author(s) 2026. CC BY 4.0 License.

Author contributions. CW configured the coupled model for the NEGIS region, conducted the simulations and wrote most parts of the manuscript. MW developed the coupling code of FESOM2-ISSM. YD, MR and MW developed the ISSM configuration used in this study. CW, RT and TK designed the study. All authors discussed the findings and contributed to the writing of the manuscript.

Competing interests. The authors declare that no competing interests are present.

Acknowledgements. We acknowledge the computational support from the Alfred Wegener Institute (AWI) high-performance computing system albedo, which was essential for the ice-sheet model initialization within the coupled FESOM2-ISSM framework. We acknowledge the computing time granted by the Resource Allocation Board and provided on the supercomputer Lise at NHR@ZIB as part of the NHR infrastructure (project hbk00099).

https://doi.org/10.5194/egusphere-2026-6782
Preprint. Discussion started: 22 November 2026
© Author(s) 2026. CC BY 4.0 License.

References

Amundson, J. M., Fahnestock, M., Truffer, M., Brown, J., Lüthi, M. P., and Motyka, R. J.: Ice mélange dynamics and implications for terminus stability, Jakobshavn Isbræ, Greenland, Journal of Geophysical Research: Earth Surface, 115, https://doi.org/10.1029/2009jf001405, 2010.

An, L., Rignot, E., Wood, M., Willis, J. K., Mouginot, J., and Khan, S. A.: Ocean melting of the Zachariae Isstrøm and Nioghalvfjerdsfjorden glaciers, northeast Greenland, PNAS, 118, https://doi.org/10.1073/pnas.2015483118, 2020.

Asay-Davis, X. S., Cornford, S. L., Durand, G., Galton-Fenzi, B. K., Gladstone, R. M., Gudmundsson, G. H., Hattermann, T., Holland, D. M., Holland, D., Holland, P. R., Martin, D. F., Mathiot, P., Pattyn, F., and Seroussi, H.: Experimental design for three interrelated marine ice sheet and ocean model intercomparison projects: MISMIP v. 3 (MISMIP +), ISOMIP v. 2 (ISOMIP +) and MISOMIP v. 1 (MISOMIP1), Geoscientific Model Development, 9, 2471–2497, https://doi.org/10.5194/gmd-9-2471-2016, 2016.

Bondzio, J. H., Seroussi, H., Morlighem, M., Kleiner, T., Rückamp, M., Humbert, A., and Larour, E. Y.: Modelling calving front dynamics using a level-set method: application to Jakobshavn Isbræ, West Greenland, The Cryosphere, 10, 497–510, https://doi.org/10.5194/tc-10-497-2016, 2016.

Brondex, J., Gagliardini, O., Gillet-Chaulet, F., and Durand, G.: Sensitivity of grounding line dynamics to the choice of the friction law, Journal of Glaciology, 63, 854–866, https://doi.org/10.1017/jog.2017.51, 2017.

Choi, Y., Morlighem, M., Rignot, E., Mouginot, J., and Wood, M.: Modeling the Response of Nioghalvfjerdsfjorden and Zachariae Isstrøm Glaciers, Greenland, to Ocean Forcing Over the Next Century, Geophysical Research Letters, 44, https://doi.org/10.1002/2017gl075174, 2017.

Choi, Y., Morlighem, M., Wood, M., and Bondzio, J. H.: Comparison of four calving laws to model Greenland outlet glaciers, The Cryosphere, 12, 3735–3746, https://doi.org/10.5194/tc-12-3735-2018, 2018.

Danilov, S., Wang, Q., Timmermann, R., Iakovlev, N., Sidorenko, D., Kimmritz, M., Jung, T., and Schröter, J.: Finite-Element Sea Ice Model (FESOM), version 2, Geosci. Model Dev., 8, 1747–1761, https://doi.org/10.5194/gmd-8-1747-2015, 2015.

Danilov, S., Sidorenko, D., Wang, Q., and Jung, T.: The Finite-volumE Sea ice–Ocean Model (FESOM2), Geoscientific Model Development, 10, 765–789, https://doi.org/10.5194/gmd-10-765-2017, 2017.

Dong, Y.-T., Zhu, H.-Y., Li, T., Zhao, J., and Shao, C.-L.: Modeling the 21st-century response of Greenland's Zachariæ Isstrøm and Nioghalvfjerdsfjorden glaciers to atmosphere–ocean forcing and friction laws, Advances in Climate Change Research, https://doi.org/10.1016/j.accre.2025.11.006, 2025.

Gardner, A., Fahnestock, M., Greene, C., Kennedy, J., Liukis, M., Lopez, L., and Scambos, T.: MEASURES ITS_LIVE Regional Glacier and Ice Sheet Surface Velocities, Version 2, NSIDC Distributed Active Center, https://doi.org/10.5067/JQ6337239C96, 2024.

Gjelstrup, C. V. B., Sejr, M. K., de Steur, L., Christiansen, J. S., Granskog, M. A., Koch, B. P., Møller, E. F., Winding, M. H. S., and Stedmon, C. A.: Vertical redistribution of principle water masses on the Northeast Greenland Shelf, Nat. Commun., 13, 7660, https://doi.org/10.1038/s41467-022-35413-z, 2022.

Gladstone, R., Galton-Fenzi, B., Gwyther, D., Zhou, Q., Hattermann, T., Zhao, C., Jong, L., Xia, Y., Guo, X., Petrakopoulos, K., Zwinger, T., Shapero, D., and Moore, J.: The Framework For Ice Sheet–Ocean Coupling (FISOC) V1.1, Geoscientific Model Development, 14, 889–905, https://doi.org/10.5194/gmd-14-889-2021, 2021.

GlaMBIE Team: Community estimate of global glacier mass changes from 2000 to 2023, Nature, 639, 382–388, https://doi.org/10.1038/s41586-024-08545-z, 2025.

https://doi.org/10.5194/egusphere-2026-6782
Preprint. Discussion started: 22 November 2026
© Author(s) 2026. CC BY 4.0 License.

Hellmer, H. and Olbers, D.: A two-dimensional model for the thermohaline circulation under an ice shelf, Antarctic Science, 1, 325–336, https://doi.org/10.1017/S0954102089000490, 1989.

Hill, E. A., Carr, J. R., and Stokes, C. R.: A Review of Recent Changes in Major Marine-Terminating Outlet Glaciers in Northern Greenland, Frontiers in Earth Science, 4, https://doi.org/10.3389/feart.2016.00111, 2017.

Holland, D. M. and Jenkins, A.: Modeling Thermodynamic Ice-Ocean Interactions at the Base of an Ice Shelf, Journal of Physical Oceanography, 29, 1787–1800, https://doi.org/10.1175/1520-0485(1999)029<1787:MTIOIA>2.0.CO;2, 1999.

Humbert, A., Helm, V., Neckel, N., Zeising, O., Rückamp, M., Khan, S. A., Loebel, E., Brauchle, J., Stebner, K., Gross, D., Sondershaus, R., and Müller, R.: Precursor of disintegration of Greenland's largest floating ice tongue, The Cryosphere, 17, 2851–2870, https://doi.org/10.5194/tc-17-2851-2023, 2023.

Jakobsson, M., Mayer, L. A., Nilsson, J., Stranne, C., Calder, B., O'Regan, M., Farrell, J. W., Cronin, T. M., Brüchert, V., Chawarski, J., Eriksson, B., Fredriksson, J., Gemery, L., Glueder, A., Holmes, F. A., Jerram, K., Kirchner, N., Mix, A., Muchowski, J., Prakash, A., Reilly, B., Thornton, B., Ulfsbo, A., Weidner, E., Åkesson, H., Handl, T., Ståhl, E., Boze, L.-G., Reed, S., West, G., and Padman, J.: Ryder Glacier in northwest Greenland is shielded from warm Atlantic water by a bathymetric sill, Communications Earth & Environment, 1, https://doi.org/10.1038/s43247-020-00043-0, 2020.

Jakobsson, M., Kirchner, N., Nilsson, J., Stranne, C., Mayer, L., Barnett, J., Holmes, F. A., Calder, B., Deutsch, C., de Boer, A. M., Coxall, H. K., Faehnrich, K., Hong, W.-L., Hopper, J. R., Ketzer, M., Noormets, R., O´Regan, M., Ross, N., Sigray, P., Erstorp, E. S., Weidner, E., and Wang, Z.: Atlantic water access and the break-up of the C.H. Ostenfeld Gletsjer ice tongue, northwest Greenland, Communications Earth & Environment, 7, https://doi.org/10.1038/s43247-026-03666-x, 2026.

Jenkins, A.: Convection-Driven Melting near the Grounding Lines of Ice Shelves and Tidewater Glaciers, Journal of Physical Oceanography, 41, 2279 – 2294, https://doi.org/10.1175/JPO-D-11-03.1, 2011.

Jesse, F., Lambert, E., Holland, P. R., Naughten, K., Berends, C., and van de Wal, R. S. W.: Meltwater pathways control the effect of subglacial discharge on sub-shelf melting, https://doi.org/10.22541/essoar.15006031/v1, 2026.

Jordan, J. R., Holland, P. R., Goldberg, D., Snow, K., Arthern, R., Campin, J., Heimbach, P., and Jenkins, A.: Ocean-Forced Ice-Shelf Thinning in a Synchronously Coupled Ice-Ocean Model, Journal of Geophysical Research: Oceans, 123, 864–882, https://doi.org/10.1002/2017jc013251, 2018.

Joughin, I., Smith, B. E., and Schoof, C. G.: Regularized Coulomb Friction Laws for Ice Sheet Sliding: Application to Pine Island Glacier, Antarctica, Geophysical Research Letters, 46, 4764–4771, https://doi.org/10.1029/2019GL082526, 2019.

Kanzow, T., Humbert, A., Mölg, T., Scheinert, M., Braun, M., Burchard, H., Doglioni, F., Hochreuther, P., Horwath, M., Huhn, O., Kappelsberger, M., Kusche, J., Loebel, E., Lutz, K., Marzeion, B., McPherson, R., Mohammadi-Aragh, M., Möller, M., Pickler, C., Reinert, M., Rhein, M., Rückamp, M., Schaffer, J., Shafeeque, M., Stolzenberger, S., Timmermann, R., Turton, J., Wekerle, C., and Zeising, O.: The system of atmosphere, land, ice and ocean in the region near the 79N Glacier in northeast Greenland: synthesis and key findings from the Greenland Ice Sheet–Ocean Interaction (GROCE) experiment, The Cryosphere, 19, 1789–1824, https://doi.org/10.5194/tc-19-1789-2025, 2025.

Khan, S. A., Choi, Y., Morlighem, M., Rignot, E., Helm, V., Humbert, A., Mouginot, J., Millan, R., Kjær, K. H., and Bjørk, A. A.: Extensive inland thinning and speed-up of Northeast Greenland Ice Stream, Nature, 611, 727–732, https://doi.org/10.1038/s41586-022-05301-z, 2022.

https://doi.org/10.5194/egusphere-2026-6782
Preprint. Discussion started: 22 November 2026
© Author(s) 2026. CC BY 4.0 License.

Krieger, L., Floricioiu, D., and Neckel, N.: Drainage basin delineation for outlet glaciers of Northeast Greenland based on Sentinel-1 ice velocities and TanDEM-X elevations, Remote Sensing of Environment, 237, 111 483, https://doi.org/https://doi.org/10.1016/j.rse.2019.111483, 2020.

Larour, E., Seroussi, H., Morlighem, M., and Rignot, E.: Continental scale, high order, high spatial resolution, ice sheet modeling using the Ice Sheet System Model (ISSM), Journal of Geophysical Research: Earth Surface, 117, https://doi.org/10.1029/2011JF002140, 2012.

Lippert, E. Y. H., Morlighem, M., Cheng, G., Berg, D. L., Hassan, J., and Khan, S. A.: Ice Front and Mélange Dynamics at Kangerlussuaq Glacier, Eastern Greenland, Since 1981, and Future Stability, Geophysical Research Letters, 52, https://doi.org/10.1029/2024gl113982, 2025.

MacAyeal, D. R.: Large-scale ice flow over a viscous basal sediment: Theory and application to ice stream B, Antarctica, Journal of Geophysical Research: Solid Earth, 94, 4071–4087, https://doi.org/10.1029/jb094ib04p04071, 1989.

Mankoff, K. D., Noël, B., Fettweis, X., Ahlstrøm, A. P., Colgan, W., Kondo, K., Langley, K., Sugiyama, S., van As, D., and Fausto, R. S.: Greenland liquid water discharge from 1958 through 2019, Earth System Science Data, 12, 2811–2841, https://doi.org/10.5194/essd-12-2811-2020, 2020a.

Mankoff, K. D., Solgaard, A., Colgan, W., Ahlstrøm, A. P., Khan, S. A., and Fausto, R. S.: Greenland Ice Sheet solid ice discharge from 1986 through March 2020, Earth System Science Data, 12, 1367–1383, https://doi.org/10.5194/essd-12-1367-2020, 2020b.

Mayer, C., Schaffer, J., Hattermann, T., Floricioiu, D., Krieger, L., Dodd, P. A., Kanzow, T., Licciulli, C., and Schannwell, C.: Large ice loss variability at Nioghalvfjerdsfjorden Glacier, Northeast-Greenland, Nature Communications, 9, https://doi.org/10.1038/s41467-018-05180-x, 2018.

McPherson, R., Wekerle, C., and Kanzow, T.: Shifts of the Recirculation Pathways in central Fram Strait drive Atlantic Intermediate Water Variability on Northeast Greenland shelf, Journal of Geophysical Research: Oceans, https://doi.org/10.1029/2023jc019915, 2023.

McPherson, R., Wekerle, C., Kanzow, T., Ionita, M., Heukamp, F., Zeising, O., and Humbert, A.: Atmospheric blocking slows ocean-driven melting of Greenland's largest glacier tongue, Science, 385, 1360–1366, https://doi.org/10.1126/science.ado5008, 2024.

Millan, R., Jager, E., Mouginot, J., Wood, M. H., Larsen, S. H., Mathiot, P., Jourdain, N. C., and Bjørk, A.: Rapid disintegration and weakening of ice shelves in North Greenland, Nature Communications, 14, https://doi.org/10.1038/s41467-023-42198-2, 2023.

Mohammadi-Aragh, M., Zeising, O., Reinert, M., Klingbeil, K., Humbert, A., McPherson, R., Morlighem, M., Timmermann, R., Wekerle, C., and Burchard, H.: Impact of Ice Topography, Basal Channels and Subglacial Discharge on Basal Melting Under the Floating Ice Tongue of 79N Glacier, Northeast Greenland, Journal of Advances in Modeling Earth Systems, 17, https://doi.org/10.1029/2024ms004735, 2025.

Morlighem, M., Williams, C. N., Rignot, E., An, L., Arndt, J. E., Bamber, J. L., Catania, G., Chauché, N., Dowdeswell, J. A., Dorschel, B., Fenty, I., Hogan, K., Howat, I., Hubbard, A., Jakobsson, M., Jordan, T. M., Kjeldsen, K. K., Millan, R., Mayer, L., Mouginot, J., Noël, B. P. Y., O'Cofaigh, C., Palmer, S., Rysgaard, S., Seroussi, H., Siegert, M. J., Slabon, P., Straneo, F., van den Broeke, M. R., Weinrebe, W., Wood, M., and Zinglersen, K. B.: BedMachine v3: Complete Bed Topography and Ocean Bathymetry Mapping of Greenland From Multibeam Echo Sounding Combined With Mass Conservation, Geophysical Research Letters, 44, https://doi.org/10.1002/2017gl074954, 2017.

Mouginot, J., Rignot, E., Scheuchl, B., Fenty, I., Khazendar, A., Morlighem, M., Buzzi, A., and Paden, J.: Fast retreat of Zachariæ Isstrøm, northeast Greenland, Science, 350, 1357–1361, https://doi.org/10.1126/science.aac7111, 2015.

Noël, B.: Rapid ablation zone expansion amplifies north Greenland mass loss: modelled (RACMO2) and observed (MODIS) data sets, https://doi.org/10.1594/PANGAEA.904428, 2019.

https://doi.org/10.5194/egusphere-2026-6782
Preprint. Discussion started: 22 November 2026
© Author(s) 2026. CC BY 4.0 License.

Noël, B., van de Berg, W. J., Lhermitte, S., and van den Broeke, M. R.: Rapid ablation zone expansion amplifies north Greenland mass loss, Science Advances, 5, https://doi.org/10.1126/sciadv.aaw0123, 2019.

Paolo, F. S., Gardner, A. S., Greene, C. A., Nilsson, J., Schodlok, M. P., Schlegel, N.-J., and Fricker, H. A.: Widespread slowdown in thinning rates of West Antarctic ice shelves, The Cryosphere, 17, 3409–3433, https://doi.org/10.5194/tc-17-3409-2023, 2023.

Reeh, N., Thomsen, H. H., Higgins, A. K., and Weidick, A.: Sea ice and the stability of north and northeast Greenland floating glaciers, Annals of Glaciology, 33, 474–480, https://doi.org/10.3189/172756401781818554, 2001.

Reinert, M., Wekerle, C., Klingbeil, K., Lorenz, M., and Burchard, H.: The multilayer ocean circulation melting the 79N Glacier ice tongue, The Cryosphere, 20, 4563–4584, https://doi.org/10.5194/tc-20-4563-2026, 2026.

Rückamp, M., Neckel, N., Berger, S., Humbert, A., and Helm, V.: Calving Induced Speedup of Petermann Glacier, Journal of Geophysical Research: Earth Surface, 124, 216–228, https://doi.org/10.1029/2018jf004775, 2019.

Schaffer, J., von Appen, W.-J., Dodd, P. A., Hofstede, C., Mayer, C., de Steur, L., and Kanzow, T.: Warm water pathways toward Nioghalvfjerdsfjorden Glacier, Northeast Greenland, Journal of Geophysical Research: Oceans, 122, 4004–4020, https://doi.org/10.1002/2016JC012462, 2017.

Schaffer, J., Timmermann, R., Arndt, J. E., Rosier, S. H. R., Anker, P. G. D., Callard, S. L., Davis, P. E. D., Dorschel, B., Grob, H., Hattermann, T., Hofstede, C. M., Kanzow, T., Kappelsberger, M., Lloyd, J. M., Ó Cofaigh, C., and Roberts, D. H.: An update to Greenland and Antarctic ice sheet topography, cavity geometry, and global bathymetry (RTopo-2.0.4), https://doi.org/10.1594/PANGAEA.905295, 2019.

Schaffer, J., Kanzow, T., von Appen, W., von Albedyll, L., Arndt, J., and Roberts, D. H.: Bathymetry constrains ocean heat supply to Greenland's largest glacier tongue, Nat. Geosci., 13, 227–231, https://doi.org/10.1038/s41561-019-0529-x, 2020.

Seroussi, H. and Morlighem, M.: Representation of basal melting at the grounding line in ice flow models, The Cryosphere, 12, 3085–3096, https://doi.org/10.5194/tc-12-3085-2018, 2018.

Steele, M., Morley, R., and Ermold, W.: PHC: a global ocean hydrography with a high-quality Arctic Ocean, J. Climate, 14, 2079–2087, https://doi.org/10.1175/1520-0442(2001)014<2079:pagohw>2.0.co;2, 2001.

Timmermann, R. and Goeller, S.: Response to Filchner–Ronne Ice Shelf cavity warming in a coupled ocean–ice sheet model – Part 1: The ocean perspective, Ocean Science, 13, 765–776, https://doi.org/10.5194/os-13-765-2017, 2017.

Tsujino, H., Urakawa, S., Nakano, H., Small, R. J., Kim, W. M., Yeager, S. G., Danabasoglu, G., Suzuki, T., Bamber, J. L., Bentsen, M., B"oning, C. W., Bozec, A., Chassignet, E. P., Curchitser, E., Boeira Dias, F., Durack, P. J., Griffies, S. M., Harada, Y., Ilicak, M., Josey, S. A., Kobayashi, C., Kobayashi, S., Komuro, Y., Large, W. G., Le Sommer, J., Marsland, S. J., Masina, S., Scheinert, M., Tomita, H., Valdivieso, M., and Yamazaki, D.: JRA-55 based surface dataset for driving ocean-sea-ice models (JRA55-do), Ocean Modelling, 130, 79–139, https://doi.org/10.1016/j.ocemod.2018.07.002, 2018.

Wekerle, C.: Model data used in the paper 'Role of ice sheet- ocean interactions in driving the current retreat of Northeast Greenland glaciers', https://doi.org/10.5281/zenodo.23861634, 2026.

Wekerle, C., McPherson, R., von Appen, W.-J., Wang, Q., Timmermann, R., Scholz, P., Danilov, S., Shu, Q., and Kanzow, T.: Atlantic Water warming increases melt below Northeast Greenland's last floating ice tongue, Nature Communications, 15, https://doi.org/10.1038/s41467-024-45650-z, 2024.

Wilner, J. A., Morlighem, M., and Cheng, G.: Evaluation of four calving laws for Antarctic ice shelves, The Cryosphere, 17, 4889–4901, https://doi.org/10.5194/tc-17-4889-2023, 2023.

https://doi.org/10.5194/egusphere-2026-6782
Preprint. Discussion started: 22 November 2026
© Author(s) 2026. CC BY 4.0 License.



Wilson, N., Straneo, F., and Heimbach, P.: Satellite-derived submarine melt rates and mass balance (2011–2015) for Greenland's largest remaining ice tongues, The Cryosphere, 11, 2773–2782, https://doi.org/10.5194/tc-11-2773-2017, 2017.

Wolovick, M., Humbert, A., Kleiner, T., and Rückamp, M.: Regularization and L-curves in ice sheet inverse models: a case study in the Filchner–Ronne catchment, The Cryosphere, 17, 5027–5060, https://doi.org/10.5194/tc-17-5027-2023, 2023.

Zeising, O., Neckel, N., Dörr, N., Helm, V., Steinhage, D., Timmermann, R., and Humbert, A.: Extreme melting at Greenland's largest floating ice tongue, The Cryosphere, 18, 1333–1357, https://doi.org/10.5194/tc-18-1333-2024, 2024.